On the Localized Transition of Pipe Poiseuille Flow. Part I: The Role of Tensile Force Flow

Yingying Yang and Huaichun Zhou *

Posted Date: 10 April 2026

doi: 10.20944/preprints202604.0699.v1

Keywords: viscous fluid flow; Reynolds numbers; laminar-turbulent transition; early turbulence; membrane force model; tensile force flow; pipe Poiseuille flow; shear stress; virtual spherical liquid layer; shear stress; high Re laminar flow

 doi:10.20944/preprints202604.0699.v1

Article

On the Localized Transition of Pipe Poiseuille Flow. Part I: The Role of Tensile Force Flow

Yingying Yang [1,2,3] and Huaichun Zhou [1,2,3,4,*]

[1] School of Low-carbon Energy and Power Engineering, China University of Mining and Technology, Xuzhou 221116, China

[2] Jiangsu Smart Energy Technology and Equipment Research Center, China University of Mining and Technology, Xuzhou 221116, China

[3] Jiangsu Provincial Center for Applied Mechanics (China University of Mining and Technology)

[4] Laboratory of Fluid and Power Machinery, Ministry of Education, Xihua University, Chengdu 610036, China

* Correspondence: hczhou@xhu.edu.cn

Abstract

The early turbulence phenomenon has been observed in pipe flow of very dilute polymer solutions [1–4], and the full chord laminar flow can be achieved on various laminar suction wings at high Reynolds numbers (*Re*) up to approximately 2 000 000 [5–7]. Their transition conditions deviate significantly from the traditional criteria, critical *Re* about 2 000~2 300, which is quoted in most contemporary textbooks for pipe flow [8–13]. In this paper, a new force model with a virtual fluid layer, which is of a hemispherical shell shape and with a constant thickness inside a laminar pipe flow is established, on the basis of the membrane force model of a spherical shell under uniformly distributed load conditions in structural mechanics. In laminar flow state with a lower *Re* and a lower pressure gradient, the curvature radius of the virtual spherical liquid layer is inversely proportional to the pressure gradient. As *Re* increases, pressure gradient also increases, while the curvature radius decreases. When the curvature radius decreases to be equal to and starting less than the pipe radius, the stable liquid layer structure collapses, and the laminar flow becomes turbulent. This is a transition state with a critical tensile force flow defined as twice the product of the viscosity of the fluid and the maximum velocity in pipe, divided by the pipe radius. In laminar flow situation, the shear stress at the pipe wall can be interpreted as a horizontal component of the critical tensile force flow, and the direction is against the flow. Only when the flow achieving the transition condition, the shear stress at the wall become the critical tensile force flow itself, which had already been observed in early turbulence [1–4,14]. The second case, which can be explained by the concept of critical tensile force flow, is high *Re* laminar pipe flow [5–7], for example, the pipe with surface suction can be considered as a part of a virtual, larger pipe with a no slip wall at where the shear stress coincides with the critical tensile force flow, the shear stress at the real pipe is smaller, with a weakening factor related to the ratio of the average velocity in the real pipe to its maximum velocity.

Keywords: viscous fluid flow; Reynolds numbers; laminar-turbulent transition; early turbulence; membrane force model; tensile force flow; pipe Poiseuille flow; shear stress; virtual spherical liquid layer; shear stress; high *Re* laminar flow

1. Introduction

Pipe flow is one of the most important topics in turbulence research [8,9], as a representative of a large category of wall-bounded flows, such as those in channels, ducts and boundary layers [13], and furthermore, the physical mechanism of laminar turbulent transition in pipe Poiseuille flow is an essential part of fluid mechanics [8,9,13]. The application of "Reynolds number" criteria has penetrated into various branches of fluid mechanics, and for pipe flow without a streamlined inlet,

 doi:10.20944/preprints202604.0699.v1

the critical value quoted in most contemporary textbooks is about 2 000~2 300 [10]. Even all theoretical and numerical investigations indicate that the flow is linearly stable, in practice, however, pipe flows are usually turbulent even at modest flow rates, and it can be concluded that there is no any critical flow rate for the onset of turbulent flow in a pipe [15]. There are two cases where their transition *Re* numbers both significantly deviate from the critical value. One is early turbulence [1,14,16], which was termed as "structural turbulence" initially [2], the criterion for the onset of turbulence was a sharp increase of apparent viscosity, and critical *Re* were found in extreme cases to be as low as 1 [2]. This phenomenon was also observed in the flow of very dilute polymer solutions in tubes with larger sizes than capillary ones1. The relationship between flow rate and wall shear stress for these solutions corresponded to the Poiseuille's Law below a certain well-defined onset wall shear stress, at which *Re* was less than the transition value for Newtonian fluids. The low *Re* or 'elastic' turbulence accompanied by significant stretching of the polymer molecules seems to belong to this case17. Polymeric drag reduction does not commence until the shear stress at the wall exceeds some critical "onset" or threshold value [3]. In the polymeric regime with drag reduction [3], the onset wall shear stress is essentially independent of pipe diameter, polymer concentration, and solvent viscosity [4,18,19]. The other case is the full chord laminar flow as well as low wing profile drags achieved at high *Re* on various laminar suction wings [5–7], where full-chord laminar flow was maintained by application of area suction up to a *Re* of approximately 2 000 000 [6]. It shows that likely from the results that attainment of full-chord laminar flow by means of continuous suction through a porous surface will not be precluded by a further increase of *Re* provided that the airfoil surfaces are maintained sufficiently smooth and fair and provided that outflow of air through the surface is prevented. The existence of the two cases above indicate that *Re* alone cannot fully determine the transition conditions from laminar to turbulent flow.

Hydrodynamic stability is studied based on the response to small disturbances [20], but there is limited research on the possible essential factors that determine the ability of laminar flow to resist from transition due to different disturbances. A possible essential factor for instance is that, a well-defined critical wall shear stress must be exceeded before early turbulence can be observed [1,14], which has not been thoroughly analyzed from a physical mechanism perspective. A membrane force model for liquid layer under capillary meniscus in cylindrical tubes has been reported by the present author group [21]. Experimental results showed that the capillary meniscus of a pure liquid inside a cylindrical tube under gravity only is probably a part of a spherical surface with a single radius of curvature, under cases of several different pipe diameters. In this paper, the membrane force model in structural mechanics [22] was inspired to establish a new force model for a virtual fluid shell with a hemispherical shell shape inside a laminar pipe flow. This new model leads to an introduction of the concept of tensile force flow, and the critical tensile force flow at transition condition. Then, the critical tensile force flow is used to explain the early turbulence phenomenon. Finally, some unique insights are proposed.

2. Derivation of Critical Tensile Force Flow in Pipe Poiseuille Flow

In membrane theory in structural mechanics, a shell structure carries a given load by pure membrane action, and no bending action occurs [22]. The bending and twisting stiffnesses of the shell are considered to be negligible compared with the membrane stiffnesses. As a thin shell structure, the plane stress components $\sigma_{\varphi\varphi}$ and $\sigma_{\theta\theta}$ (with dimensions of force per unit area), where φ and ϑ refer to the meridian and circumferential directions respectively, not only are the only active stresses but also are constantly distributed over the thickness of the membrane. This perspective leads to the concept of force flows, i.e., $N_{\varphi\varphi}$ and $N_{\vartheta\vartheta}$, which are obtained by multiplying the plane stress components by the shell thickness, h, namely $N_{\varphi\varphi}$=$\sigma_{\varphi\varphi}h$, $N_{\vartheta\vartheta}$=$\sigma_{\vartheta\vartheta}h$. As a result, the dimension of force flows is force per unit length, which is identical to the dimension of surface tension.

For a hemispherical shell under a load q uniformly distributed over the planform, as shown in Figure 1(a), the surface load is expressed as [22] $P_\varphi = qcos\varphi sin\varphi$, $P_Z = -qcos^2\varphi$, and the distributions of the membrane force flows $N_{\varphi\varphi}$ and $N_{\vartheta\vartheta}$ are given as: $N_{\varphi\varphi} = -\frac{qR}{2}$, $N_{\vartheta\vartheta} =$

 doi:10.20944/preprints202604.0699.v1

$-\frac{1}{2}qRcos2\varphi$. The profiles of $N_{\varphi\varphi}$ and $N_{\vartheta\vartheta}$ are given in Figure 1(a). Obviously, $N_{\varphi\varphi}$, independent from the angle φ, is a constant value of $-\frac{qR}{2}$ along the meridian direction, but for $N_{\vartheta\vartheta}$, the value varies along the circumferential direction and a sign change occurs at $\varphi = 45°$ [22].

In a recent work by the present author group[21], a membrane force model for liquid layer under capillary meniscus in cylindrical tubes has been reported. If the weight of the liquid layer with a constant height beneath the capillary meniscus is considered as a load, the Young-Laplace surface tension is exactly the same as the meridian membrane force flow inside a spherical shell with uniformly distributed loads on the planform. Experimental results had shown that a complete capillary meniscus of the pure liquid inside a cylindrical tube under the action of gravity is very close to a part of a spherical surface with a single radius of curvature, regardless of the pipe diameter. So, any virtual liquid layer in a capillary tube can be regarded as a membrane from the perspective of structural mechanics, and the forces in the membrane are only axial forces (tension or compression), with no bending moments, torques, or shear forces. In present paper, the membrane force model is applied to analyze the fluid force in laminar flow.

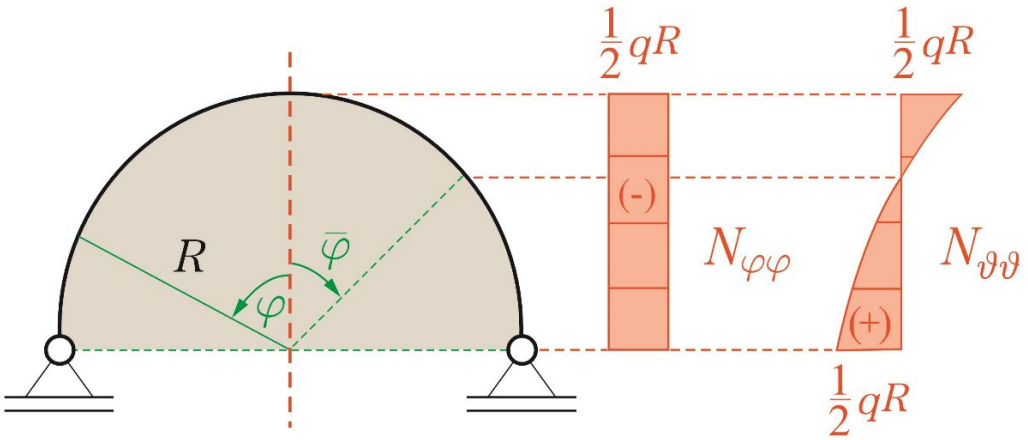

(**a**)

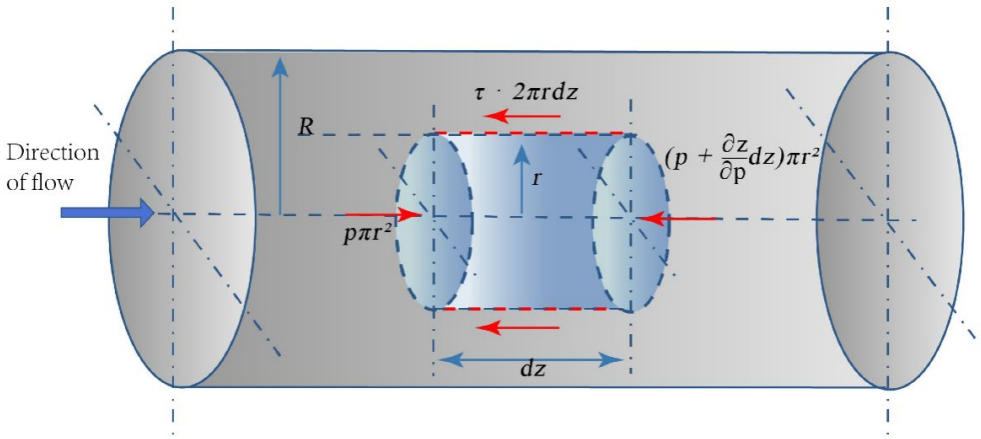

(**b**)

Preprints.org (www.preprints.org) | NOT PEER-REVIEWED | Posted: 10 April 2026 doi:10.20944/preprints202604.0699.v1

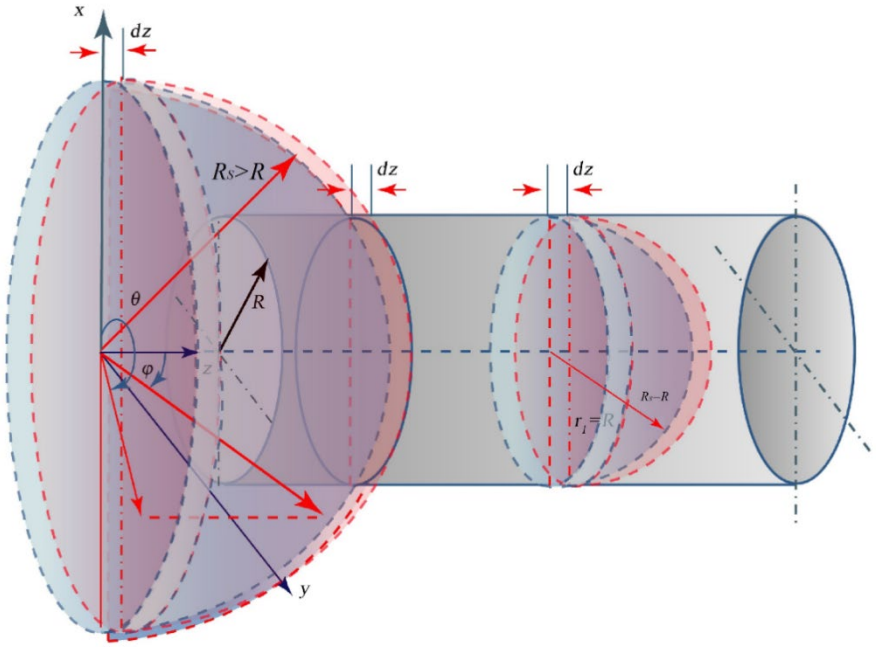

(**c**)

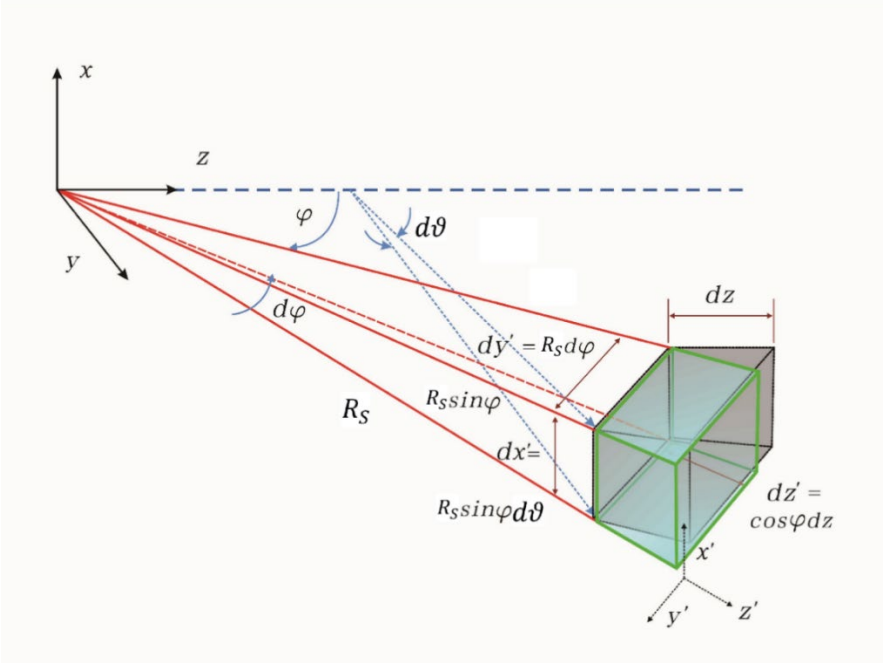

(**d**)

Figure 1. Laminar hemispherical fluid layers in pipe and the microelement for force analysis. (**a**) A hemispherical shell under a load q uniformly distributed over the planform. The distributions of the membrane force flows $N_{\varphi\varphi}$ and $N_{\vartheta\vartheta}$ are given as: $N_{\varphi\varphi} = -\frac{qR}{2}$, $N_{\vartheta\vartheta} = -\frac{qRcos2\varphi}{2}$. (**b**) Steady laminar and incompressible flow through pipe. [23] The velocity direction is set to be the z direction. The flow is laminar: $u_r = u_\vartheta = 0$, $u_z = u_0\left(1 - \frac{r^2}{R^2}\right)$, $u_0 = -\frac{R^2}{4\mu}\frac{\partial p}{\partial z}$, where $\frac{\partial p}{\partial z} < 0$. The shear stress at $r = R$ is $\tau_w = \mu\frac{du}{dr}\Big|_{r=R} = -\frac{2\mu u_0}{R}$. (**c**) Hemispherical-shell-shaped fluid layers with thickness of dz in flow direction. R_S is the single curvature radius of the virtual layer, $R_S \geq R$, where the subscript S means 'spherical'. (**d**) A differential element of a hemispherical shell in local $x'y'z'$ coordinates, where $dz' = cos\varphi dz$, $dx' = rd\vartheta = R_S sin\varphi d\vartheta$, $dy' = R_S d\varphi$. The force flows in the x' and y' coordinates correspond to $\gamma_{\vartheta\vartheta}$ and $\gamma_{\varphi\varphi}$, and the pressure in the z'-direction is $\sigma_{z'} = p(z)$.

 doi:10.20944/preprints202604.0699.v1

The laminar, incompressible and steady flow through pipe, as shown in Figure 1(b), can be completely analyzed by two Laws: (i) Newton's Law of viscosity and (ii) Newton's Second Law of motion [23]. In this case, the force balance is achieved between the pressure difference force of the two ends of the fluid element, and the shear forces acting on the side surface of the element opposing the motion (acting from right to left), as shown in Figure 1(b). The velocity direction is set to be in the z direction. The viscosity of fluid in this case is a constant, and the flow is laminar: $u_r = u_\vartheta = 0$, $u_z = u_0\left(1-\frac{r^2}{R^2}\right)$, $u_0 = -\frac{R^2}{4\mu}\frac{\partial p}{\partial z}$, where $\frac{\partial p}{\partial z} < 0$. The average velocity is $u = \frac{u_0}{2}$. The shear stress at $r = R$ is $\tau_w = \mu\frac{du}{dr}\Big|_{r=R} = -\frac{2\mu u_0}{R}$. The negative sign indicates the negative direction of z axis.

If the cylindrical object is rigid, it is easy to understand the balance between the force acting on the side and the forces acting on the two ends. But in this case shown in Figure 1(b), the fluid element is not a rigid body; even if we can apply the axioms of rigidization in theoretical mechanics to the reformable body in Figure 1(b) in the steady state [24]. We need to find other analysis method for the force equilibrium.

If we consider a hemispherical-shell-shaped fluid layer in the direction of flow in Figure 1(c) with thickness of dz, the pressure difference force across the circular cross-sectional layer is $\frac{\partial p}{\partial z}dz$, and its dimension is force per unit surface area, which can be regarded as a load, namely $q = -\frac{\partial p}{\partial z}dz$. Then, the hemispherical shell membrane force flow model is applicable in this case. The meridian membrane force flow is $N_{\varphi\varphi} = \frac{qR_S}{2} = -\frac{R_S}{2}\frac{\partial p}{\partial z}dz$, where R_S is the curvature radius of the virtual, hemispherical liquid layer. Since $u_0 = -\frac{R^2}{4\mu}\frac{\partial p}{\partial z}$, then the membrane force flows are: $N_{\varphi\varphi} = \frac{R_S}{2}\frac{\partial p}{\partial z}dz = \frac{R_S}{2}\frac{4\mu u_0}{R^2}dz = \frac{2R_S\mu u_0}{R^2}dz$, and $N_{\vartheta\vartheta} = \frac{2R_S\mu u_0}{R^2}cos2\varphi dz$.

We define

$$\gamma_\nu = \gamma_{\varphi\varphi} = \frac{N_{\varphi\varphi}}{dz} = \frac{2R_S\mu u_0}{R^2}, \quad (1)$$

Then

$$\gamma_{\vartheta\vartheta} = \frac{N_{\vartheta\vartheta}}{dz} = \frac{2R_S\mu u_0}{R^2}cos2\varphi = \gamma_\nu cos2\varphi, \quad (2)$$

where, γ_ν is the tensile force flow, a new kind of force flow with unit of N/m² for the fluid layer. $\gamma_{\varphi\varphi}$ and $\gamma_{\vartheta\vartheta}$ are the new force flows along the directions of φ and ϑ, respectively. The symbol, γ, is borrowed from the surface tension coefficient, and the subscript ν corresponds to the dynamic viscosity of fluid. The unit of γ_ν is identical with that of the shear stress, and we can see the difference between these two later.

As shown in Figure 1(d), a liquid microelement in the local rectangular coordinate system with $dx' = R_S sin\varphi d\vartheta$, $dy' = R_S d\varphi$, and $dz' = cos\varphi dz$. Its volume is $R_S^2 sin\varphi cos\varphi d\vartheta d\varphi dz$. An important issue needed to be explained here is that the local rectangular $x'y'z'$ coordinate system at any microelement is uniquely fixed, which is only determined by local axial forces (presenting as pressure or tension), in directions of meridian and ring, without effects from any bending moments, torques, or shear forces. The stresses acting on a liquid microelement in dx', dy', and dz' directions are $\sigma_{x'}$, $\sigma_{y'}$, and $\sigma_{z'}$, and they are internal forces in material mechanics.

According to Equation (1), the curvature radius R_S of the liquid layer is proportional to γ_ν, and inversely proportional to $\frac{\partial p}{\partial z}$,

$$R_S = \frac{R^2\gamma_\nu}{2\mu u_0} = -\frac{2\gamma_\nu}{\frac{\partial p}{\partial z}}. \quad (3)$$

Since $u_0 = -\frac{R^2}{4\mu}\frac{\partial p}{\partial z}$, when the flow velocity is low, the pressure difference force is small, and the virtual spherical shell radius is larger than the geometric pipe radius. This corresponds to the virtual, hemispherical shell on the left in Figure 1(c), $R_S \geq R$. In an extreme situation when flow velocity is zero and pressure difference force is zero, the radius of the virtual hemispherical shell is infinitely large. As the pressure difference force increases, Re increases, while the curvature radius R_S of the liquid layer of the virtual spherical shell decreases. When R_S decreases to being equal to or less than the geometric pipe radius, the stable liquid layer in laminar flow collapses, and the laminar flow

 doi:10.20944/preprints202604.0699.v1

becomes turbulent. This situation may be illustrated by the smaller virtual hemispherical shell on the right in Figure 1(c), where $R = R_S$. In this case,

$$R = R_S = -\frac{2R^2\gamma_v}{\frac{\partial p}{\partial z}} = \frac{R^2\gamma_v}{2\mu u_0}. \quad (4)$$

We have

$$\gamma_v = \frac{2\mu u_0}{R_S} = \frac{2\mu u_0}{R}. \quad (5)$$

The value of γ_v is equal to that of the critical shear stress when $R = R_S$, as $\tau_w = -\frac{2\mu u_0}{R}$. It means that for a certain fluid, the maximum radius, R, of a pipe in which the fluid motion remains laminar is proportional to the velocity of the fluid, u_0. This is a conclusion drawn out from the shell-shaped, membrane force flow model, surprisingly inconsistent with the trend predicted by Reynolds number, $R_e = \frac{\rho R u_0}{\mu}$. According to Reynolds number criterion, it is clear that for a very large velocity u_0 and a very small radius R, the flow state can remain similar and laminar. However, from the perspective of the membrane force model, this is impossible. With a very large velocity u_0 and a very small diameter, $D = 2R$, i.e., to keep *Re* number the same, the flow state can not remain laminar, and it is easy for the thin liquid layer to be torn by the excessive load, under which it cannot withstand.

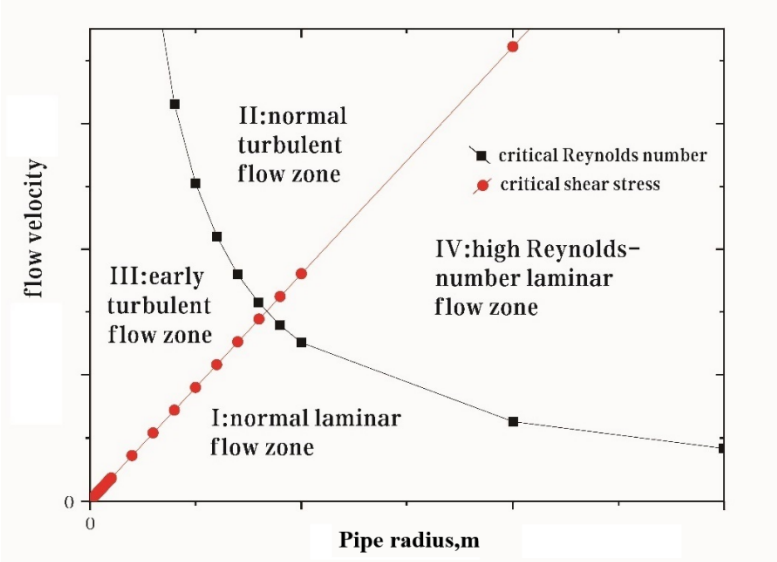

(**a**)

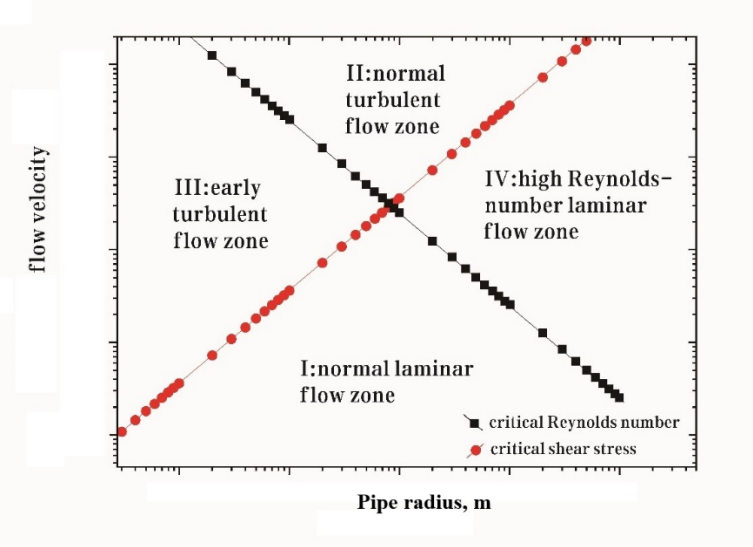

(**b**)

 doi:10.20944/preprints202604.0699.v1

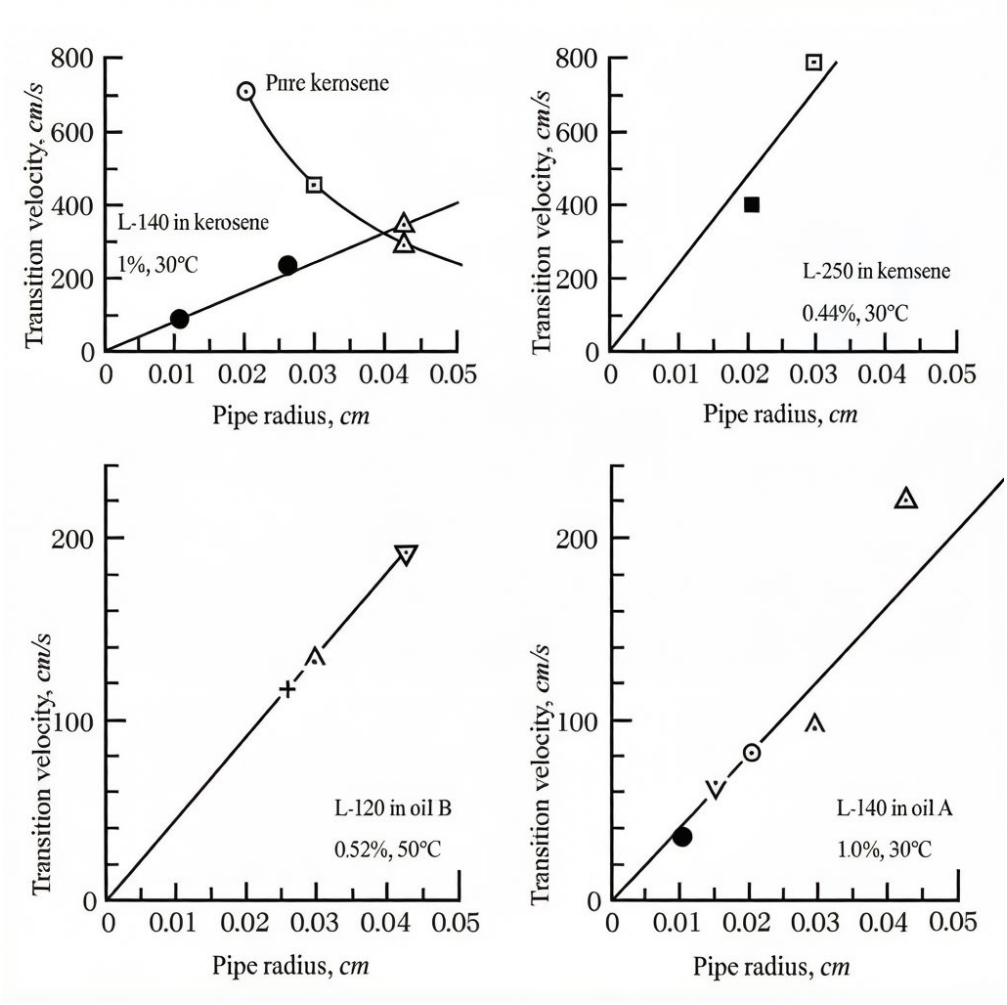

(**c**)

Figure 2. The relationship between the transition velocity of lamina flow and the radius of pipe. (**a**) The two possible relationships between transition velocity and pipe radius. One is that the transition velocity is proportional to the pipe radius, deviated from the present work, while the other one is deduced by the critical Reynolds number. Two lines cut the whole domains into four zones, I, II, III and IV. In zone I, the flow is laminar. In zone II, the flow is turbulent. In zone III, the flow should be laminar according to the *Re* number, while it was observed as early turbulence from experiments [2]. In zone IV, the flow should be turbulent by Re number criterion, while it may be laminar through experiments [5] with high Re number, by surface suction for example. (**b**) Four zones in (**a**) illustrated in logarithmic coordinates. (**c**) The relationship between critical transition velocity and pipe radius of the various polymer solutions, which was called as structural turbulence, or early turbulence, was plotted in Figure 7 of literature, and reproduced here with permission [2]. Structural turbulence is characterized by a critical shear stress, resulting in the critical velocity versus the capillary radius described by a straight line extrapolated to the origin. It was stated that this critical shear stress indicates a collapse of the structure of the fluid [2].

Until now, we get that for a certain fluid, the maximum radius of the pipe in which the fluid motion remain laminar is proportional to the velocity of the fluid, as given by Equation (5), and the critical Reynolds number gives $R_{e,c} = \frac{\rho R u_0}{\mu}$. The relationship between the transition velocity of laminar flow and the radius of pipe is demonstrated in Figure 2a,b. In this figure, four zones can be identified. If we use the critical Reynolds number to distinguish between laminar and turbulent flows, zones I and II belong to laminar flow, and zones III and IV belong to turbulent flow. If we use a critical tensile force flow by Equation (5) to distinguish between laminar and turbulent flows, zones II and III belong to laminar flow, and zones I and IV belong to turbulent flow. Regions II and IV are identified as laminar and turbulent flows, respectively, by both the two methods. However, zones I

 doi:10.20944/preprints202604.0699.v1

and III are identified as two domains with completely opposite properties by the two methods, the critical tensile force flow method to distinguish between laminar and turbulent flows is obviously more consistent with the two types of flow phenomena introduced at the beginning of the present paper, and will be explained later in detail.

3. Two Types of Flow Phenomena Explained by the Critical Tensile Force Flow

3.1. Early Turbulence

Zone III in Figure 2a,b belongs to the so-called early turbulence, or structural turbulence region introduced initially [2], and a conclusion was drawn out that structural turbulence is characterized by a critical shear stress, which has a certain value for each substance, and this *critical shear stress* (in this article, it is actually the *critical tensile force flow*) indicates a collapse of the structure of the fluid. In Figure 2(c), which is the Figure 7 of [2] reproduced here after permission, the difference between critical-Reynolds-number and structural turbulence criteria is clearly visualized. On plotting the transition velocity versus the pipe radius, structural turbulence is described by a straight line extrapolated to the origin, as shown in Figure 2(c), being obviously predicted in Figure 2a,b. The turbulence characterized by *Re*, on the other hand, is characterized by a hyperbolic curve. It was further concluded that the critical Reynolds number loses its significance as a criterion for structural turbulence[2], and that structural turbulence is generally detected only in pipes of small diameter where the high shear stresses needed to produce the effect can be reached below the transition Reynolds number for Reynolds turbulence [25]. It was suggested that the wall shear stress which characterizes the onset of structural turbulence is roughly independent of tube diameter [2,25]. This statement confirms that the tensile force flow γ_v is a property parameter of a fluid.

3.2. High-Reynolds-Number Laminar Flow

The phenomenon of the so-called full chord laminar flow maintained up to a *Re* of approximately 20×10^6 [5–7] corresponds to zone IV in Figure 2a,b, and can be explained by a conceptual model shown in Figure 3.

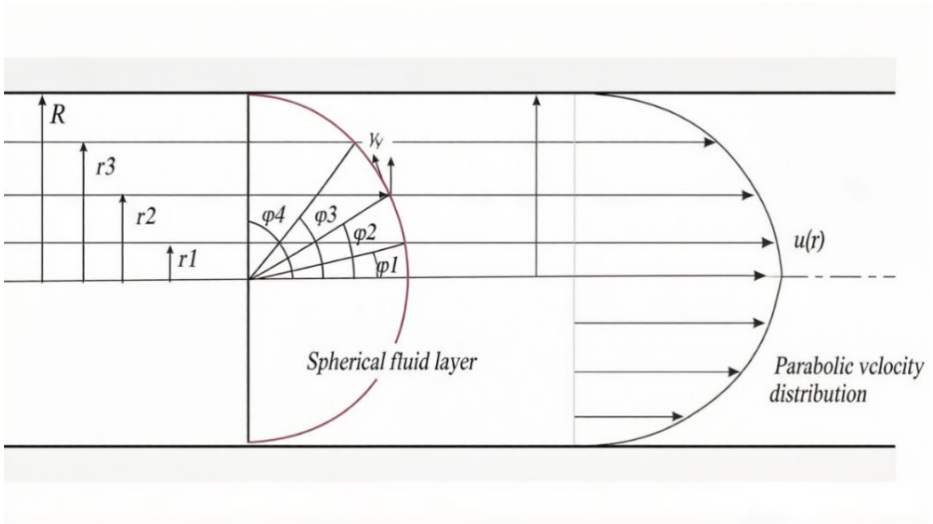

(**a**)

 doi:10.20944/preprints202604.0699.v1

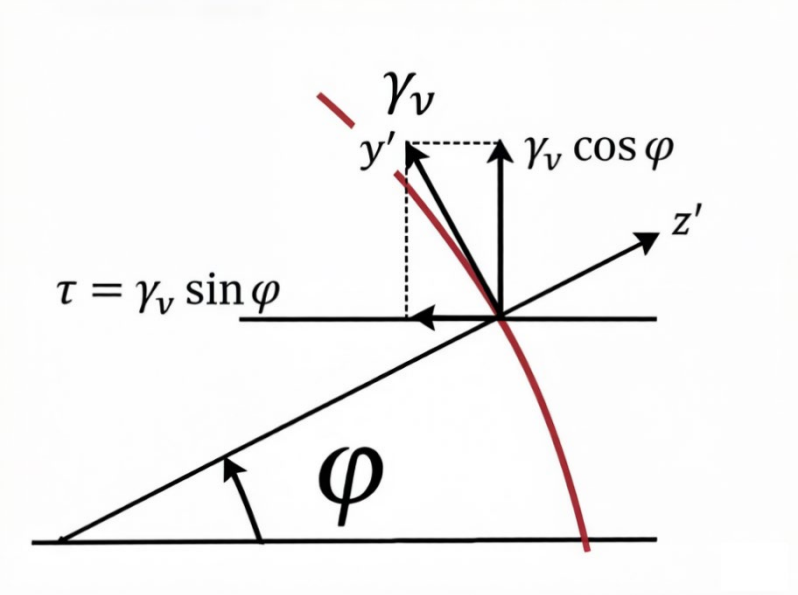

(**b**)

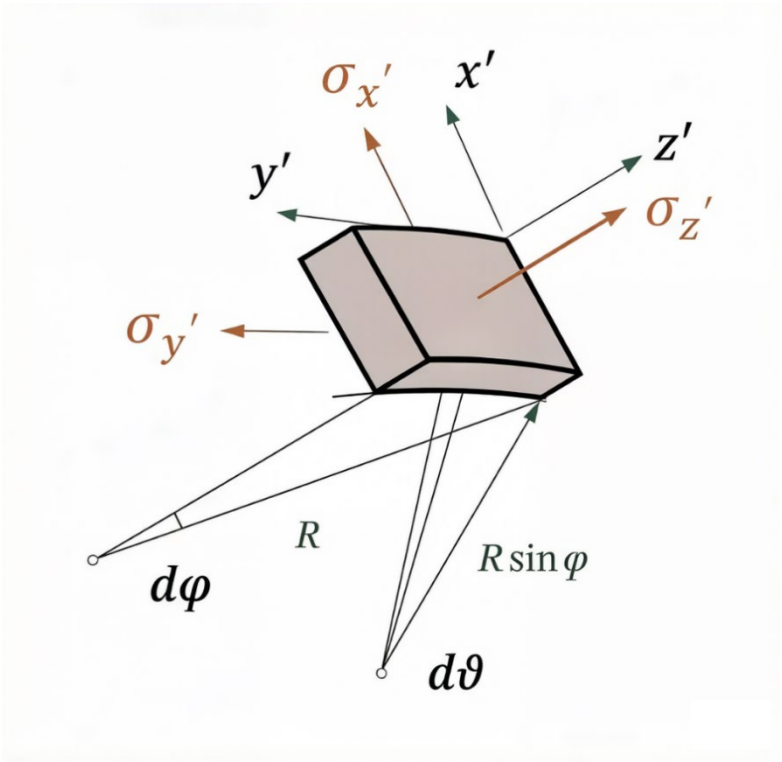

(**c**)

Figure 3. The conceptual model for high-Reynolds-number laminar flow. (**a**) The flow inside a pipe with no slip at the wall in a transition state, and its hemispherical shell fluid layer has a spherical shell radius of R_S equal to the pipe radius R. Supposing that a high Reynolds number laminar pipe flow with a smaller radius r can be considered as a partial flow inside this pipe. (**b**) The shear stress τ is a component of the tensile force flow γ_v along the flow direction. The shear stress within the smaller pipe becomes $\tau = \gamma_v sin\varphi$. If $\varphi = 90°$, the shear stress at wall ($r = R = R_S$) becomes $\tau_{w,c} = \gamma_v$. (**c**) A microelement in the local $x'y'z'$ system as shown in Figure 3C, where $\sigma_{x'}, \sigma_{y'}$ are related to γ_v, respectively, and $\sigma_{z'} = p(z)$.

It is show in Figure 3a that the flow inside a pipe with no slip at the wall in a transition state, and its spherical shell fluid layer has a spherical shell radius equal to the pipe radius, $R = R_S$. Supposing that a high-Reynolds-number laminar flow can be considered as a partial flow with a small radius $r < R = R_S$. For the velocity profile $u_z = u_0\left(1 - \frac{r^2}{R^2}\right)$, the fluid velocity near to the tube wall at

 doi:10.20944/preprints202604.0699.v1

$r < R_S$, u_r, can be expressed as $u_r = u_0 cos^2\varphi$. The shear stress near to the tube wall at $r < R_S$, as shown in Figure 3(b), becomes

$$\tau = \gamma_v sin\varphi. \quad (6)$$

By surface suction, the shear stress near to the wall decreases by a factor of $sin\varphi$, indicating a drag-reduction effect. The significance of the equation above is reflected in the fact that for the same fluid, under the same pipe radius, the higher the fluid velocity near to the wall through any means such as surface suction, the lower the wall shear stress near to the pipe wall as the laminar flow state is maintained.

It is easy to estimate the average flow velocity within $r < R = R_S$, which is

$$\overline{u}' = \frac{u_0}{R^2}\left(R^2 - \frac{r^2}{2}\right). \quad (7)$$

So, if the average velocity $\overline{u}'$ of the full chord laminar flow is known, the angle φ can be calculated out as

$$\sin\varphi = \sqrt{2\left(1 - \frac{\overline{u}'}{u_0}\right)}. \quad (8)$$

The Reynolds number of up to approximately 20×10⁶ [5–7] for the so-called full chord laminar flow is calculated from $R_{e,c} = \frac{2\rho r\overline{u}'}{\mu}$. The data with completely laminar flow through the entire pipe for Runs 1, 2 and 3 of the first series of experiments [5] are adopted to proceed, and the results are given in Table 1, together with data from the second and third series of experiments. The length *Re* has not been considered here. We can get u_0 from $\overline{u}'$ and $\frac{u_0}{\overline{u}'}$ in reference[5], and since $\overline{u}'/u_0 = \frac{1}{R^2}\left(R^2 - \frac{r^2}{2}\right)$, we can get the virtual radius $R = R_S$, as given in Table 1. As $\sin\varphi$ is got from $\overline{u}'/u_0$, then φ is obtained. It can be seen that most of φ are around 45°, which approaches the angle from where the change of sign for $N_{\vartheta\vartheta}$ occurs as shown in Figure 1(a) [22]. We guess that it is related to the localization of onset of the transition, and will be treated in the next paper in near future. We can get a virtual *Re* for the whole flow within $R = R_S$, which is $R_{e,virtual} = \rho R u_0/\mu$, as shown in Table 1. It can be seen that $R_{e,virtual}$ approaches $R_{e,c}$, since the virtual radius is larger than the original radius, and the average speed is of opposite trend. The critical tensile force flow γ_v is given in Table 1. From the five lines of data [5], except for the fourth line of data, γ_v varies slightly around 0.040, showing a certain stability as a characteristic parameter. The shear stress at the real wall τ, is less than γ_v by Equation (6). As shown in Figure 3(b), τ is a component of γ_v, and only as φ =90°, they become the same. The concept of viscous shear vector proposed by the corresponding author of present paper will be beneficial for further analysis on the force balance in fluids [26].

Table 1. Calculation of flow parameters for virtual pipe from the original data [5].

r (m)	$\overline{u}'$	$\frac{\overline{u}'r}{\nu}$	$\frac{u_0}{\overline{u}'}$	Re	u_0	sinφ	φ(°)	$R(m)$	virtual *Re*	$\overline{u}$	γ_v	τ
0.0254	30.5	50050	1.3	100100.0	39.8	0.68	43	0.037	95580	19.9	0.041	0.028
0.0254	26.66	44200	1.3	88400.0	35.9	0.72	46	0.035	82919	18.0	0.039	0.028
0.0254	25.04	41470	1.4	82940.0	35.0	0.75	49	0.034	76845	17.5	0.040	0.030
0.0128	51.3	44000	1.5	88000.0	77.2	0.82	55	0.016	80834	38.6	0.184	0.151
0.0254	30	49600	1.4	99200.0	42.3	0.76	50	0.033	91707	21.2	0.049	0.037

4. Conclusions

This article discusses the force structure of laminar flow in a pipe and proposes a flow transition mechanism from laminar to turbulent. The research conclusions are as follows:

(1) Considering that the pressure difference force acting as the driving force for fluid motion in a circular tube is uniformly distributed at the cross-section of the tube, the force model of a fluid layer with a certain thickness and spherical shell shape inside the tube is established by the membrane force model of a spherical shell under uniformly distributed load conditions in structural mechanics. The radial force flow can be quantitatively expressed from the product of the pressure difference load and the spherical shell radius R_S.

 doi:10.20944/preprints202604.0699.v1

(2) As *Re* increases, the pressure difference force also increases, while the curvature radius R_S of the liquid layer of the virtual, spherical shell decreases. When R_S decreases to be equal to or less than the geometric radius of the circular tube *R*, the stable liquid layer in laminar flow collapses and the laminar flow becomes turbulent. Under this condition, a critical tensile force flow is deduced as $\gamma_v = \frac{2\mu u_0}{R}$.

(3) The critical tensile force flow is a constant, and is a property for the fluid. Shear stress is a component of the critical tensile force flow against the flow direction. Only when the flow achieves the transition condition, the shear stress at the wall is equal to the critical tensile force flow, which has been observed in early turbulence as in literature [1–4,14].

(4) The physical mechanism for the so-called full chord laminar flow [5–7] by surface suction for example, which is maintained up to a *Re* of approximately 20×10^6 can be explained by the concept of critical tensile force flow. The shear stress near to the tube wall decreases by a factor of $sin\varphi$, while this tube is considered as part of a virtual, larger tube which has a non-slip wall condition, and the shear stress at the virtual wall is equal to the critical tensile force flow.

The next step of the work is to establish a new viscous fluid motion equation based on the stresses and their distribution inside a general fluid motion.

Author Contributions: H.Z. proposed the concept, Y.Y. and H.Z. performed the theoretical analysis and wrote the manuscript. All authors have reviewed and discussed the results in the manuscript.

Funding: Y.Y. acknowledge the financial support from Special Project for the Construction of Research Bases (Interdisciplinary Research on Frontiers of Applied Mechanics) of the Fundamental Research Funds for the Central Universities, China University of Mining and Technology under Grant No. 2024KYJD1013, and H.Z. acknowledges the financial support from the National Natural Science Foundation of China under Grant No. 51827808, High-level Talent Introduction Plan of Xihua University under Grant No. ZX20250126.

Conflicts of Interest: The authors declare no competing interests.

References

1. Forame, P.C.; Hansen, R.J.; Little, R.C. Observations of early turbulence in the pipe flow of drag reducing polymer solutions. *AIChE J.* **1972**, *18*, 213–217. https://doi.org/10.1002/aic.690180139.
2. Ram, A.; Tamir, A. Structural turbulence in polymer solutions. *J. Appl. Polym. Sci.* **1964**, *8*, 2751–2762. https://doi.org/10.1002/app.1964.070080621.
3. Manfield, P. D., Lawrence, C. J. & Hewitt, G. F. Drage Reduction with Additives in Multiohase Flow: a Literature Survey. Multiphase Science and Technology 11, 197-221 (1999).
4. Virk, P.S. Drag reduction fundamentals. *AIChE J.* **1975**, *21*, 625–656. https://doi.org/10.1002/aic.690210402.
5. Pfenninger, W. Boundary Layer Suction Experiments with Laminar Flow at High Reynolds Numbers in the Inlet Length of a Tube by Various Suction Methods. Boundary Layer and Flow Control, Its Principles and Application, 961-980 (1961). https://doi.org:10.1016/B978-1-4832-1323-1.50013-0
6. Braslow, A. L. & Visconti, F. Further experimental studies of area suction for the control of the laminar boundary layer on a porous bronze NACA 64A010 airfoil. (National Advisory Committee for Aeronautics, 1950).
7. Braslow, A. L., Burrows, D. L., Tetervin, N. & Visconti, F. Experimental and Theoretical Studies of Area Suction for the Control of the Laminar Boundary Layer on an NACA 64A010 Airfoil. (National Advisory Committee for Aeronautics, 1951).
8. Eckert, M. Pipe flow: a gateway to turbulence. *Arch. Hist. Exact Sci.* **2020**, *75*, 249–282. https://doi.org/10.1007/s00407-020-00263-y.
9. Avila, M.; Barkley, D.; Hof, B. Transition to Turbulence in Pipe Flow. *Annu. Rev. Fluid Mech.* **2023**, *55*, 575–602. https://doi.org/10.1146/annurev-fluid-120720-025957.
10. Rott, N. Note On The History Of The Reynolds Number. *Annu. Rev. Fluid Mech.* **1990**, *22*, 1–11. https://doi.org/10.1146/annurev.fluid.22.1.1.

 doi:10.20944/preprints202604.0699.v1

11. Reynolds, O. An Experimental Investigation of the Circumstances which Determine whether the Motion of Water shall be Direct or Sinuous, and of the Law of Resistance in Parallel Channels. Philosophical Transactions of the Royal Society of London (1883).
12. Reynolds, O. IV. On the dynamical theory of incompressible viscous fluids and the determination of the criterion. *Philos. Trans. R. Soc. London. (A.)* **1895**, *186*, 123–164. https://doi.org/10.1098/rsta.1895.0004.
13. Barkley, D. Theoretical perspective on the route to turbulence in a pipe. *J. Fluid Mech.* **2016**, *803*. https://doi.org/10.1017/jfm.2016.465.
14. Hansen, R.J.; Little, R.C.; Forame, P.G. EXPERIMENTAL AND THEORETICAL STUDIES OF EARLY TURBULENCE. *J. Chem. Eng. Jpn.* **1973**, *6*, 310–314. https://doi.org/10.1252/jcej.6.310.
15. Mullin, T. Experimental Studies of Transition to Turbulence in a Pipe. *Annu. Rev. Fluid Mech.* **2011**, *43*, 1–24. https://doi.org/10.1146/annurev-fluid-122109-160652.
16. Hansen, R.J.; Little, R.C. Early turbulence and drag reduction phenomena in larger pipes. *Nature* **1974**, *252*, 690–690. https://doi.org/10.1038/252690a0.
17. Groisman, A.; Steinberg, V. Elastic turbulence in a polymer solution flow. *Nature* **2000**, *405*, 53–55. https://doi.org/10.1038/35011019.
18. Virk, P. S. The Toms Phenomenon-Turbulent Pipe Flow of Dilute Polymer Solutions Degree of Doctor of Seience thesis, Massachuseits Institute of Technology, (1966).
19. Virk, P. S., Merrill, E. W., Mickley, H. S. & Smith, K. A. in International Conference on Rheology (ed S Eskinazi) 37-52 (Academic Press, Pinebrook Conference Center of Syracuse University, Pinebrook, New York, USA, 1965).
20. Boiko, A. V., Dovgal, A. V., Grek, G. R. & Kozlov, V. V. Physics of Transitional Shear Flows: Instability and Laminar–Turbulent Transition in Incompressible Near-Wall Shear Layers. Vol. 98 (Springer Science+Business Media B.V., 2012).
21. Guo, H.; Li, K.; Yang, Y.; Yu, B.; Zhou, H. High precision measurement of meniscus profile on liquid column in cylindrical capillary based on telecentric imaging technology. *Opt. Express* **2025**, *33*, 41364–41378. https://doi.org/10.1364/oe.572866.
22. Mittelstedt, C. *Theory of Plates and Shells*; Springer Nature: Durham, NC, United States, 2023; ISBN: .
23. Shiv Kumar. Fluid Mechanics (Vol. 2) - Basic Concepts and Principles. Fourth Edition edn, (Springer, 2023).
24. Zhang, J. Theoretical Mechanics. (Northwestern Polytechnical University Press, 2018).
25. Little, R.C.; Wiegard, M. Drag reduction and structural turbulence in flowing polyox solutions. *J. Appl. Polym. Sci.* **1970**, *14*, 409–419. https://doi.org/10.1002/app.1970.070140215.
26. Zhou, H.-C. Does shear viscosity play a key role in the flow across a normal shock wave? *Therm. Sci.* **2024**, *28*, 126–126. https://doi.org/10.2298/tsci230328126z.